



Parametric Amplification and Cascaded-Nonlinearity Processes in Common Atomic System

Huaibin Zheng, Xun Zhang, Zhaoyang Zhang, Yaling Tian, Haixia Chen, Changbiao Li & Yanpeng Zhang

Key Laboratory for Physical Electronics and Devices of the Ministry of Education & Shaanxi Key Lab of Information Photonic Technique, Xi'an Jiaotong University, Xi'an 710049, China.

SUBJECT AREAS:
QUANTUM OPTICS
NONLINEAR OPTICS
ATOM OPTICS
FLUORESCENCE SPECTROMETRY

Received
6 March 2013

Accepted
7 May 2013

Published
24 May 2013

Correspondence and
requests for materials
should be addressed to

C.L. (cbli@mail.xjtu.
edu.cn) or Y.Z.
(ypzhang@mail.xjtu.
edu.cn)

For the first time, we study the parametric amplification process of multi-wave mixing (PA-MWM) signal and cascaded-nonlinearity process (CNP) in sodium vapors both theoretically and experimentally, based on a conventional phase-conjugate MWM and a self-diffraction four-wave mixing (SD-FWM) processes, which are pumped by laser or amplified spontaneous emission (ASE), respectively. For laser pumping case, SD-FWM process serves as a quantum linear amplifier (a CNP) out (inside) of the resonant absorption region. While for ASE case, only the CNP occurs and the output linewidth is much narrower than that of the MWM signal due to the second selected effect of its electromagnetically induced transparency window. In addition, the phase-sensitive amplifying process seeded by two MWM processes is discussed for the first time. Theoretical fittings agree well with the experiment. The investigations have important potential applications in quantum communication.

The so-called cascaded-nonlinearity process (CNP) is comparable to or has higher value than direct higher-order nonlinear process. Such processes are widely studied in non-centrosymmetric materials, where the cascaded second-order process plays an important role in the intrinsic third-order response for some effects¹. Recently, microscopic cascaded third-order process contribution to the fifth-order nonlinear susceptibility has been experimentally observed in a liquid cell containing a mixture of CS₂ and C₆₀². In our previous work³, we experimentally showed how cascaded third-order nonlinear optical processes were generated in a four-level inverted-Y atomic system. Such efficient cascaded four-wave mixing (FWM) processes can coexist with the direct six-wave mixing (SWM) process in the system with controllable relative strengths. Thus, one can get a more efficient higher-order multi-wave mixing (MWM) signal by cascading two lower-order nonlinear processes, which can be analyzed separately even though they coexist with each other.

Recent progresses in intensity squeezed light with FWM in an atomic vapor, have applications in producing linear phase-insensitive as well as phase-sensitive amplifiers (PIA, PSA)^{4,5}, preparing multi-spatial-mode entangled beams, precision measurements beyond the shot-noise limit (SNL), noise-free imaging, and improved position to quantum information processing⁶. In contrast to the second-order nonlinear process occurring in nonlinear crystal, FWM process has narrower bandwidth due to phase-matching condition. The “double- Λ ” FWM process introduced by Mc Cormick et al applies a high intensity “pump” beam to drive a cycle of four off-resonant transitions in a hot rubidium vapor⁷, inducing the emission of correlated Stokes and anti-Stokes photons. When the process is not seeded, the output state is the two-mode squeezed vacuum. The instantaneous electric fields of the output Stokes and anti-Stokes lights are zero on average, but have quantum-correlation in fluctuations.

The nonlinear process mentioned above can be used as a linear PIA or PSA by carefully setting the experimental parameters^{4,5}, because a large third-order nonlinear susceptibility can result in a large single-pass gain without a cavity. And what interest us is that they add as little noise as possible to the signal they amplify. The most common optical amplifier is the PIA, which amplifies both the quadrature that carries the signal and the conjugate quadrature that carries only noise. When a weak input probe is seeded on the Stokes channel and no input conjugate on the corresponding anti-Stokes channel, the power of the probe will be amplified by a factor $\Omega = \cosh^2 r$ while the quantum-correlated conjugate beam by $\Omega - 1$. In contrast, PSA amplifies both the signal and the noise in the quadrature that carries information but deamplifies the noise in the conjugate quadrature that does not carry information⁸. Specially, the ability to implement a PSA that can simultaneously amplify multiple-spatial-mode allows noiseless image amplification⁵. The multi-spatial-mode nature arises from the relaxed



phase-matching conditions of the FWM, making it possible to amplify a wide range of probe wave vectors. These properties are also the basis of the FWM-based PIA in Ref. 7. The spatial bandwidth of PSA is characterized by the input and output spatial modes and their associated phase-sensitive gains under focused-beam pumping. The number of independent optical modes that can be coupled in the medium depends on geometrical parameters⁹. The smallest detail that can be imprinted on the output beams far away from the nonlinear medium is limited by diffraction off the finite-sized gain region which is inversely proportional to the transverse size of the pump beam.

In this paper, the parametric amplification process of MWM (PA-MWM) signal and CNP are theoretically and experimentally investigated in a sodium vapor for the first time to our best knowledge. Phase conjugate MWM as well as self-diffraction FWM (SD-FWM) processes pumped by laser or amplified spontaneous emission (ASE) are considered. For laser pumping, the SD-FWM process can serve as a quantum linear amplifier or a CNP corresponding to outside or inside the resonant absorption linewidth, respectively. For the ASE pumping case, only the CNP occurs. In the two cases, the linewidth of the MWM signal of the “first” process has the same magnitude due to the selected effect of its electromagnetically induced transparency (EIT) window while that of the “second” process is much narrower than the corresponding result of the “first process” due to the second selected effect of its EIT window. In addition, the PSA process seeded by two MWM processes and CNP constituted of a SWM process and a FWM process are investigated for the first time.

Results

The parametric amplification process can be viewed as a special case of the CNP, that is, one SD-FWM process serving as a linear amplifier amplifies the other coexisting FWM signal as shown in Fig. 1. The seeded FWM signal E_F can be obtained from three incident beams E_1 , E_2 , and E'_2 . A SD-FWM process occurred in a “double- Λ ” configuration coupled by E_1 and two generated beams respectively named as Stokes beam E_S and anti-Stokes beam E_{aS} is used to be a linear amplifier^{4,5} as shown in Fig. 1(b). E_F is injected into the Stokes channel as shown in the schematic in Fig. 1.

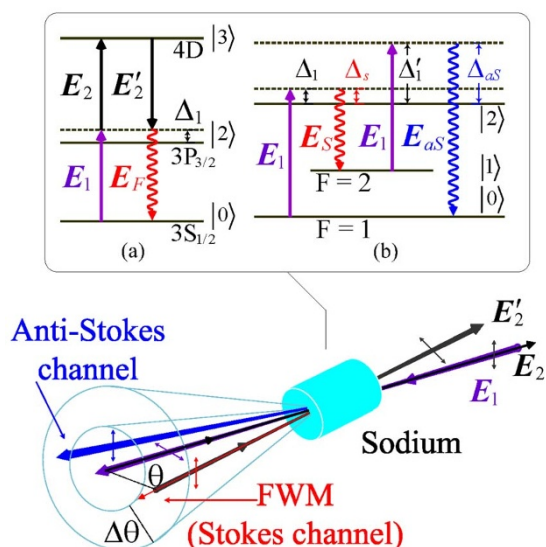


Figure 1 | The schematic of the FWM OPA process, where E_F is seeded into the channel of E_S . (a) A phase-conjugate FWM process with phase-matching condition $\mathbf{k}_F = \mathbf{k}_1 + \mathbf{k}_2 - \mathbf{k}'_2$ in a ladder-type three-level atomic system. (b) A SD-FWM process occurring in a “double- Λ ” configuration coupled by E_1 , generated Stokes beam E_S and anti-Stokes beam E_{aS} .

Theoretically, the seeded FWM signal E_F can be described by the perturbation chain $\rho_{00}^{(0)} \xrightarrow{\omega_1} \rho_{20}^{(1)} \xrightarrow{\omega_2} \rho_{30}^{(2)} \xrightarrow{-\omega_2} \rho_{20(F)}^{(3)}$ by means of the Liouville pathway¹⁰, and the corresponding density matrix element can be written as

$$\rho_{FWM}^{(3)} = -iG_1 G_2 G_2^* / (d_{20}^2 d_{30}), \quad (1)$$

where $G_i = \mu_i E_i / \hbar$ ($i = 1, 2$) is the Rabi frequency, $d_{20} = \Gamma_{20} + i\Delta_1$, $d_{30} = \Gamma_{30} + i(\Delta_1 + \Delta_2)$, and Γ_{ij} is the decay rate.

By blocking driving beams E_2 and E'_2 as shown in Fig. 1(b), the so-called conical emission⁷ is observed. Such process is well interpreted by a SD-FWM process, in which a strong pumping field E_1 is mixed with two weak fields E_S and E_{aS} , satisfying $\mathbf{k}_S = 2\mathbf{k}_1 - \mathbf{k}_{aS}$ and $\mathbf{k}_{aS} = 2\mathbf{k}_1 - \mathbf{k}_S$, respectively. With this configuration, the coherence between the two ground states is built, which enhances the efficiency of the FWM process¹¹. Quantum mechanically, such process (off-resonant FWM) can be viewed as a linear amplifier with properties of either PIA⁴ or PSA⁵ by carefully setting the experimental parameters such as frequency detuning, power of each incident beam and so on. This amplifier involves coupled Stokes channel and anti-Stokes channel, and produces twin photons. One can express this coupling with the Hamiltonian

$$H = \frac{g}{v} (\hat{a}^+ \hat{b}^+ + \hat{a} \hat{b}), \quad (2)$$

where \hat{a}^+ (\hat{a}) is the boson-creation (-annihilation) operator that acts on the electromagnetic excitation of the Stokes channel, whereas \hat{b}^+ (\hat{b}) acts on the anti-Stokes channel. v is the group velocity of the light in the nonlinear medium, and $g = |\chi^{(3)} \mathbf{E}_1 \mathbf{E}_1| = |N \mu_{10}^2 \rho_{s/as}^{(3)} / \hbar \epsilon_0 G_{s/as}|$ is the pumping parameter of the amplifier, which depends on the nonlinearity $\chi^{(3)}$ and the pump-field amplitude. Different from the case occurring in nonlinear crystal, $\chi^{(3)}$ is a function of the density matrix elements which can be described by the perturbation chains $\rho_{11}^{(0)} \xrightarrow{\omega_1} \rho_{21}^{(1)} \xrightarrow{\omega_{as}} \rho_{01}^{(2)} \xrightarrow{\omega_1} \rho_{21(S)}^{(3)}$ (Stokes signal) and $\rho_{00}^{(0)} \xrightarrow{\omega_1} \rho_{20}^{(1)} \xrightarrow{\omega_2} \rho_{10}^{(2)} \xrightarrow{\omega_1} \rho_{20(as)}^{(3)}$ (anti-Stokes signal). We obtain

$$\rho_{21(S)}^{(3)} = -iG_{aS}^* G_1^2 / (d_{21} d'_{10} d'_{21}), \quad (3)$$

$$\rho_{20(as)}^{(3)} = -iG_S^* G_1^2 / (d_{20} d_{10} d'_{20}), \quad (4)$$

where, $d_{21} = \Gamma_{21} + i\Delta_1$, $d_{10} = \Gamma_{10} + i(\Delta_1 - \Delta_S)$, $d'_{10} = \Gamma_{10} + i(\Delta_1 - \Delta_{aS})$, $d'_{20} = \Gamma_{20} + i(2\Delta_1 - \Delta_S)$, $d'_{21} = \Gamma_{21} + i(2\Delta_1 - \Delta_{aS})$. When light propagates in the nonlinear medium it evolves under the Hamiltonian of the system, the numbers of photons measured at each channel are

$$\langle \hat{a}_{out}^+ \hat{a}_{out} \rangle = \frac{1}{2} \left[\cos\left(2t\sqrt{AB} \sin \frac{\varphi_1 + \varphi_2}{2}\right) + \cosh\left(2t\sqrt{AB} \cos \frac{\varphi_1 + \varphi_2}{2}\right) \right] \frac{A}{B}, \quad (5)$$

$$\langle \hat{b}_{out}^+ \hat{b}_{out} \rangle = \frac{1}{2} \left[\cos\left(2t\sqrt{AB} \sin \frac{\varphi_1 + \varphi_2}{2}\right) + \cosh\left(2t\sqrt{AB} \cos \frac{\varphi_1 + \varphi_2}{2}\right) \right] \frac{B}{A}, \quad (6)$$

where, for conveniently, we set $\rho_{21(S)}^{(3)} = A e^{i\varphi_1}$ and $\rho_{20(as)}^{(3)} = B e^{i\varphi_2}$, A , B , φ_1 , and φ_2 are the modulus and phase angles of $\rho_{21(S)}^{(3)}$ and $\rho_{20(as)}^{(3)}$, respectively. Therefore, the gain of each channel has the same value at the output of the amplifier without seeding any signals is

$$\Omega = \frac{1}{2} \left[\cos\left(2t\sqrt{AB} \sin \frac{\varphi_1 + \varphi_2}{2}\right) + \cosh\left(2t\sqrt{AB} \cos \frac{\varphi_1 + \varphi_2}{2}\right) \right], \quad (7)$$

Such FWM process has many key properties to the successful generation of entangled beams and entangled images. First, the nonlinear gain Ω is high enough to ensure a large degree of squeezing



of the joint quadratures. Second, the scheme has been theoretically¹² and experimentally¹³ shown to be largely free of competing processes such as fluorescence, Raman gain, and so forth, which add noise and mask the squeezing. Finally, the FWM naturally operates in a multi-spatial-mode regime that means more than one pair of optical modes for the probe and conjugate beams can couple in the medium¹⁴.

When all incident beams are open, the coexisting E_F seeding into the Stokes channel of this amplifier can be amplified in an appropriate condition with phase-matching condition $\mathbf{k}_{aS} = 2\mathbf{k}_1 - \mathbf{k}_F$. The perturbation chain should be corrected as $\rho_{00}^{(0)} \xrightarrow{\omega_1} \rho_{20}^{(1)} \xrightarrow{\omega_F} \rho_{10}^{(2)} \xrightarrow{\omega_1} \rho_{20(aS)}^{(3)}$ (anti-Stokes signal) and the density matrix element in Eq. (4) is rewritten as:

$$\rho_{20(aS)}^{(3)} = -iG_F^* G_1^2 e^{i\Delta k_{as}r} / (d_{20}d_{10}d'_{20}), \quad (8)$$

where $G_F \propto \sqrt{2/\epsilon_0 \hbar N} \mu^2 \rho_{FWM}^{(3)}$. Consequently, due to the photon number of seeded signal $n \gg 1$, at the output of such PIA the numbers of photons measured at each channel are

$$\langle \hat{a}_{out}^+ \hat{a}_{out} \rangle = \frac{1}{2} \left[\cos\left(2t\sqrt{AB} \sin \frac{\varphi_1 + \varphi_2}{2}\right) + \cosh\left(2t\sqrt{AB} \cos \frac{\varphi_1 + \varphi_2}{2}\right) \right] |\alpha|^2, \quad (9)$$

$$\langle \hat{b}_{out}^+ \hat{b}_{out} \rangle = \frac{1}{2} \left[\frac{B}{A} \cosh\left(2t\sqrt{AB} \cos \frac{\varphi_1 + \varphi_2}{2}\right) - \cos\left(2t\sqrt{AB} \sin \frac{\varphi_1 + \varphi_2}{2}\right) \right] |\alpha|^2, \quad (10)$$

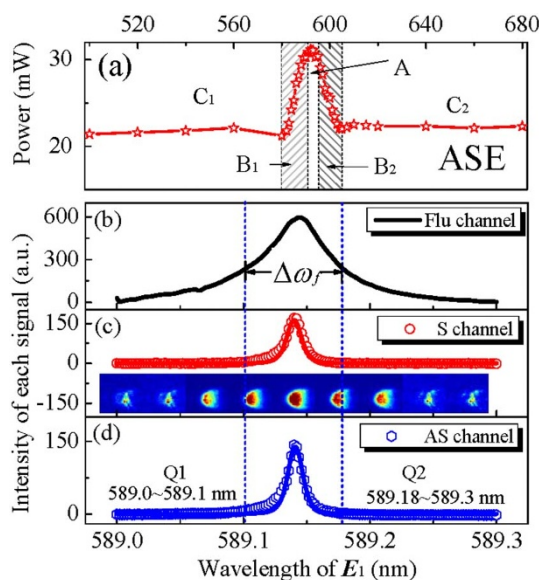


Figure 2 | (a) Curve with stars shows the power spectrum of E_1 , where A denotes the near resonant region (589.0 ~ 589.6 nm) of sodium D lines; B_1 and B_2 are the gain regions, which is far away from A; C_1 and C_2 are ASE regions where the cavity of laser does not work. By blocking fields E_2 and E'_2 , the lower panel shows the measured signals versus Δ_1 from (b) fluorescence channel, (c) Stokes channel, and (d) anti-Stokes channel around D2 line transition (Fig. 1(b)). The inset is output patterns at nine discrete frequency detuning Δ_1 . The linewidth, $\Delta\omega_f$, of the fluorescence spectrum profile at full-width at half-maximum is about 0.076 nm. Regions labeled by Q1 and Q2 are out of the effectively absorbed region, where the competing process is largely free.

where $|\alpha|^2 = (\pi\epsilon_0 \hbar / 2\omega_1)(rG_F / \mu_{10})^2$ denotes the intensity of the seeded field, r is the radius of laser beam E_F . Thus, the gains of each channel can be calculated as

$$\Omega_S = \frac{1}{2} \left[\cos\left(2t\sqrt{AB} \sin \frac{\varphi_1 + \varphi_2}{2}\right) + \cosh\left(2t\sqrt{AB} \cos \frac{\varphi_1 + \varphi_2}{2}\right) \right] \quad (11)$$

$$\Omega_{aS} = \frac{1}{2} \frac{B}{A} \left[\cos\left(2t\sqrt{AB} \sin \frac{\varphi_1 + \varphi_2}{2}\right) + \cosh\left(2t\sqrt{AB} \cos \frac{\varphi_1 + \varphi_2}{2}\right) \right]. \quad (12)$$

In addition to the case of quantum amplifier, in nonlinear optics, the CNP which is comparable with or higher in value than direct higher-order nonlinear process will be occurred at certain experiment condition, which is also one of our concerns because it possesses the same generating process as the one mentioned above. The mimic fifth-order nonlinear process caused by cascaded third-order nonlinear process ($\chi_F^{(3)}$ & $\chi_{as}^{(3)}$) can be expressed by Eq. (8), that is, $\rho_{CF}^{(3)} = \rho_{20(aS)}^{(3)} = -iG_F^* G_1^2 / (d_{20}d_{10}d'_{20})$. As a result, we get the quantum amplifying case and CNP together in one system.

Figure 2(a) shows the power spectrum of E_1 by scanning the grating of the dye laser in a wide-range (The detailed experiment procedure are presented in Methods). We divide the whole curve into three regions: A denotes the near resonant region (589.0 ~ 589.6 nm) of sodium D lines, B (B_1 and B_2) the gain region, and C (C_1 and C_2) the ASE region where the cavity of laser does not work.

Firstly, we focus on the region A, where the field E_1 is scanned around the D2 line of Na atom without fields E_2 and E'_2 as shown in Fig. 1(b). Figures 2(b)–(d) show the measured intensities versus Δ_1 from the fluorescence channel, Stokes channel, and anti-Stokes channel, respectively. The linewidth ($\Delta\omega_f$) of the fluorescence spectrum profile at full-width at half-maximum (FWHM) is about 0.076 nm (~65.7 GHz), which corresponds to the absorption. Meanwhile, the linewidths of the Stokes and anti-Stokes signals (Details of such SD-FWM can be seen in Methods) at FWHM are the same, 0.021 nm (~18 GHz), which are much narrower due to the atomic coherence and parametric process. Distinctly revealing the quantum property of the system, regions labeled by Q1 and Q2 in Fig. 2(d), which are out of the effectively absorbed region, are interesting for us to demonstrate a parametric amplifier. In addition, such FWM process besides of Q1 and Q2 regions will occur more efficiently, but the quantum property mentioned above is destroyed. However, the CNP (Details are presented in Methods) can be realized easily due to large nonlinear susceptibility.

When fields E_2 and E'_2 are open, by scanning Δ_2 around the near resonant transition $|2\rangle - |3\rangle$ (568.8 nm) with different Δ_1 , a series of parametric amplification process (regions of Q1 and Q2) and CNP (the rest region inside of the linewidth $\Delta\omega_f$) are shown in Figs. 3(a) and 3(b). First, we focus on the amplifying process in regions Q1 and Q2. With Δ_1 fixed at 589.23 nm, the condition of quantum limited amplifier⁴ is satisfied because the linewidth of fluorescence spectrum is about 0.05 nm (43 GHz) away from the adjacent edge, and the amplified FWM signal E_F and corresponding anti-Stokes signal are shown in Fig. 3. As a demonstration, we block E_2 or E'_2 , and find signals from both Stokes and anti-Stokes channels disappear (not shown in figure) simultaneously, that agree with the corresponding points (589.23 nm) shown in Figs. 2(c) and 2(d). With this fact, the gain of this amplifier is $\Omega = 1.06$ in present experimental condition. Next, we turn to the region inside the linewidth of fluorescence spectrum in which the quantum properties (such as quantum correlation) of amplifier are destroyed due to strengthening of the competing processes (such as spontaneous emission). However, there has a large nonlinear susceptibility at resonance with little absorption due to EIT configuration (satisfying $\Delta_1 - \Delta_2 = 0$). Therefore, CNP

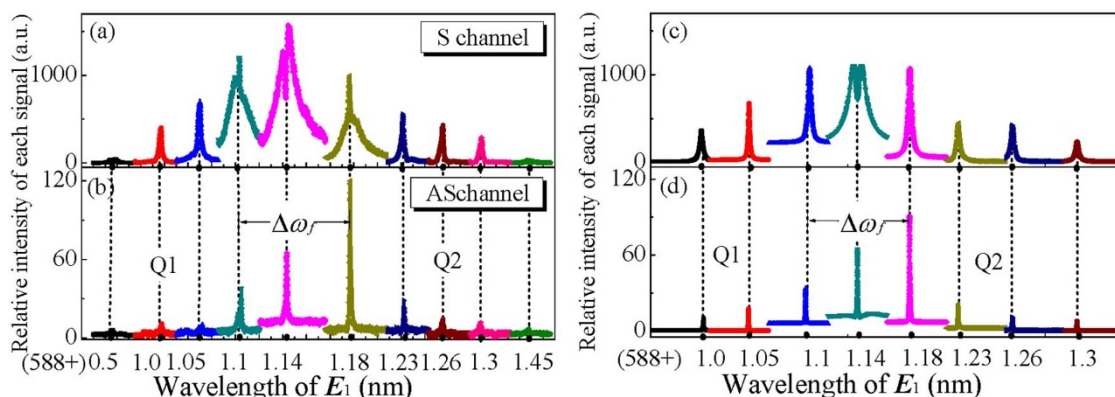


Figure 3 | Measured signals versus Δ_2 with different fixed values Δ_1 from (a) Stokes channel seeded by E_F generated in Fig. 1(a); and (b) anti-Stokes channel. Q1 and Q2 correspond to the ones presented in Fig. 2. The rest region is inside of the linewidth $\Delta\omega_f$ (c) and (d) are theoretical simulations of (a) and (b), respectively, according to the Eqs. (1), (8), (9) and (10).

will occur easily in this region due to the robust FWM process E_F . Signals from these two channels are observed, which can be attributed to the CNP. The inference is further verified by the fact that the signals from both channels disappear simultaneously with E_2 or E'_2 blocked. It is obvious that the “second” FWM spectrum (E_{CF}) is much narrower than the “first” one (E_F), because the first one experiences the power broadening and sub-Doppler broadening, while the second one experiences a second EIT selection in “double- Λ ” system (satisfying $\Delta_1 - \Delta_f = 0$). In a word, in the case of the transition $|0\rangle - |2\rangle$, one can realize either an amplifying process or a mimic higher-order nonlinear process by means of two nonlinear processes with appropriate experiment parameters. Figures 3(c) and 3(d) show the corresponding theoretical results that agree well with the experiment.

Secondly, we move to the regions labeled by B and C as shown in Fig. 2. In the region B, due to the frequency of laser field is far away from the D lines transition of sodium atom, the laser component (E_{1L}) of beam E_1 does not act on the atom any more. However, the interaction between ASE component (E_{1A}) and atom becomes dominant gradually as the frequency is far away from the maximum conversion point (~ 591.0 nm), that is, the ratio of the residual E_{1A} after conversion process for laser oscillation becomes larger and larger. Until arriving at the region C where the grating detunes too large to make the cavity work normally, the ratio of E_{1A} gets its maximum. So, there is only ASE component in E_1 in these regions.

Measured by the same method as mentioned in Fig. 3, Figs. 4 (a) and 4(c) of the first panel show the ASE-FWM (E_{FA}) occurred in the regions B and C, where E_{1L} discussed in Fig. 3 is replaced by E_{1A} . First, in the region B, the tendency profile constituted by the intensities of E_{FA} represents an evolution process of the ratio of E_{1A} , which reflects that E_{1A} becomes larger and larger as discussed above. The linewidth of FWM spectrum E_{FA} has the same order with that in region A, which can be attributed to the selected results of the resonant property of transition and the narrow bandwidth property of driving laser beams. Meanwhile, the corresponding cascaded-FWM processes with a narrower linewidth are observed in the same evolution tendency as shown in Figs. 4(b) and 4(d) of the first panel. Second, in the region C, no matter what kinds of values of Δ_1 we set, the observed E_{FA} and cascaded-FWM processes no longer present new phenomena in contrast to the adjacent edge next to the region B where the intensity of ASE beam keeps a constant. Therefore, in these regions, only the CNP is different from the one at near resonance. The corresponding theoretical results shown by the right panels of Fig. 4 agree well with the experiment.

Finally, there exists a special case in region A when E_1 is tuned to the D1 transition ($|0\rangle - |4\rangle$) and renamed as E_4 (see Fig. 5(a)), while E_2 and E'_2 are still around $|2\rangle - |3\rangle$ (568.8 nm). The “first” FWM process shown in Fig. 5(b) is generated by ASE-FWM process. But, the “second” FWM process occurs in V-type three-level atomic

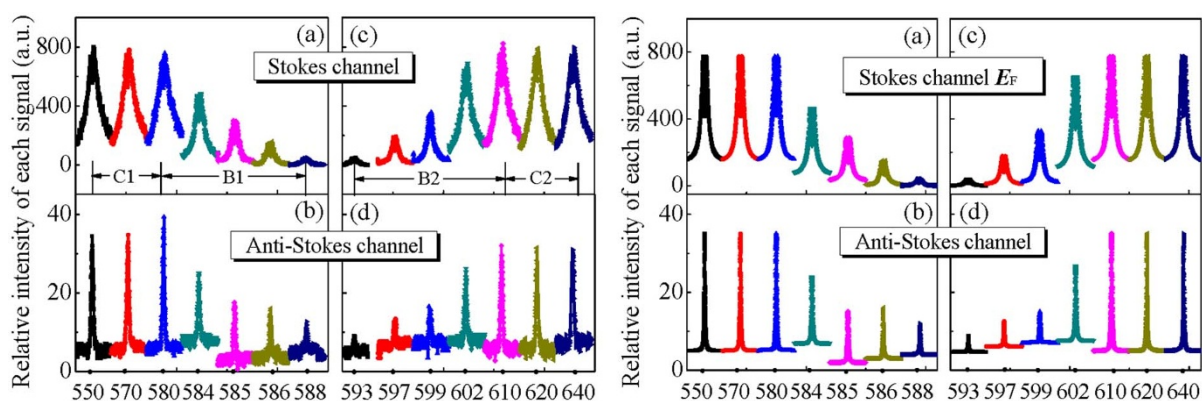


Figure 4 | The first panel: Measured cascaded-nonlinear signals from Stokes channel (a) and (c) and anti-Stokes channel (b) and (d) in the regions B and C shown in Fig. 2, where B denotes the frequency of E_1 far away from the near resonant region (589.0 ~ 589.6 nm) of sodium D lines and C is the ASE region where the cavity of laser does not work. Only the ASE component of pumping beam E_1 participates in these two FWM processes, so the generated FWM is called ASE-FWM. The second panel: theoretical simulations correspond to the first panel based on Eqs. (1) and (8).

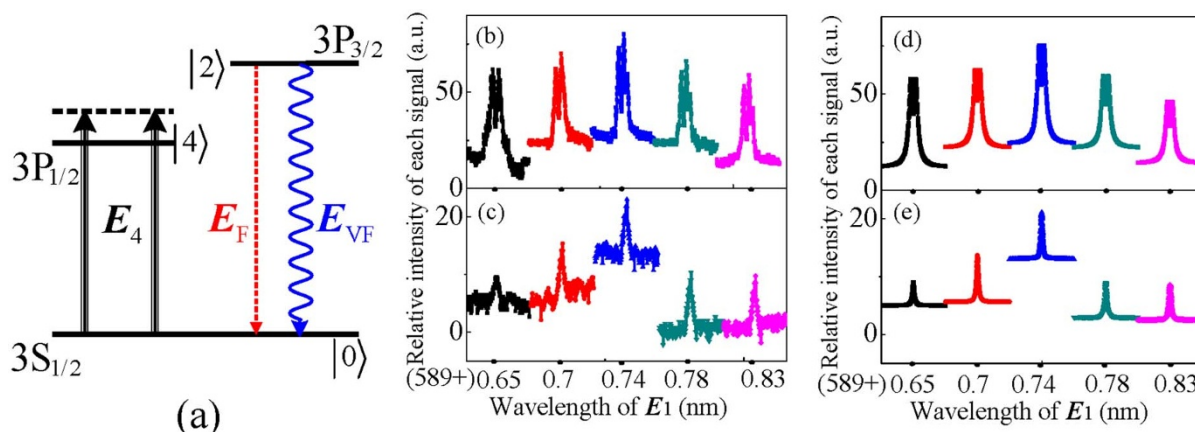


Figure 5 | (a) A dominant process of CNP occurs in V-type three-level atomic system in region A when E_1 is turned to the D1 line transition, where the CNP occurring in regions B and C is too weak to observe. (b) Measured ASE-FWM signal in Stokes channel and (c) cascaded-FWM signal in anti-Stokes channel. (d) and (e) are the corresponding theoretical simulations based on Eq. (13).

system as shown in Fig. 5(a), which has more robust efficiency than the one shown in region B. So, the V-type three-level FWM process is dominant in CNP, for which the perturbation chain is $\rho_{00}^{(0)} \xrightarrow{\omega_4} \rho_{40}^{(1)} \xrightarrow{-\omega_4} \rho_{00}^{(2)} \xrightarrow{\omega_F} \rho_{20}^{(3)}$ and the corresponding density matrix element can be written as

$$\rho_{VFWM}^{(3)} = -iG_4 G_4^* G_F / (\Gamma_{00} d_{40} d_{20}), \quad (13)$$

where $d_{40} = i\Delta_4 + \Gamma_{40}$. Figures 5(d) and 5(e) give the theoretical results of Eq. (13), which has a good agreement with the experiment.

Discussion

So far, we have presented the quantum limited amplifying process as well as CNP at resonant region and ASE region by means of two FWM process. The essential of the whole process is that there coexist two nonlinear processes which can be cascaded by carefully designing the optical layout according to the phase-matching condition of each process. As an extension to our discussion, six-wave mixing (SWM) can be also treated as the “first” nonlinear process. Even more, in the case of quantum limited amplifier, there are two seeding signals and one of which is generated in the third nonlinear process. When they are respectively seeded into the corresponding Stokes and anti-Stokes channels, such linear amplifier can be used as PSA by carefully controlling the phase of them⁵.

To realize the above proposals, two new beams E_3 and E'_3 are added onto E_2 and the opposite direction of anti-Stokes channel, respectively. By blocking beam E'_2 , one can obtain a SWM signal E_{SWM} in anti-Stokes channel satisfying $\mathbf{k}_{SWM} = \mathbf{k}_1 + \mathbf{k}_2 - \mathbf{k}_2 + \mathbf{k}_3 - \mathbf{k}'_3$. By the perturbation chain $\rho_{00}^{(0)} \xrightarrow{\omega_1} \rho_{20}^{(1)} \xrightarrow{\omega_2} \rho_{30}^{(2)} \xrightarrow{-\omega_3} \rho_{40}^{(3)} \xrightarrow{\omega_3} \rho_{30}^{(4)} \xrightarrow{-\omega_2} \rho_{20}^{(5)}$, one gets the density matrix element corresponding to the SWM signal as

$$\rho_{SWM}^{(5)} = \rho_{20}^{(5)} = -iG_1 |G_2|^2 G_3 G'_3 / (d_{20}^2 d_{30}^2 d'_{40}), \quad (14)$$

where $d'_{40} = i(\Delta_1 + \Delta_2 - \Delta_3) + \Gamma_{40}$. Substituting the FWM process, this fifth-order nonlinear process participates in the second nonlinear process with the anti-Stokes channel seeded.

When all incident beams are open, there coexist one FWM signal and one SWM signal propagating in the Stokes and anti-Stokes channels, respectively. In the case of the second FWM process serving as a linear amplifier, such seeding process by two MWM signals can be considered as PSA and the numbers of photons measured at each output channel are

$$\begin{aligned} \langle \hat{a}_{out}^+ \hat{a}_{out} \rangle &= \frac{1}{2} \left[\cos \left(2t\sqrt{AB} \sin \frac{\varphi_1 + \varphi_2}{2} \right) \right. \\ &\quad \left. + \cosh \left(2t\sqrt{AB} \cos \frac{\varphi_1 + \varphi_2}{2} \right) \right] |\alpha|^2 \\ &\quad + \frac{A}{B} \frac{1}{2} \left[\cosh \left(2t\sqrt{AB} \cos \frac{\varphi_1 + \varphi_2}{2} \right) \right. \\ &\quad \left. - \cos \left(2t\sqrt{AB} \sin \frac{\varphi_1 + \varphi_2}{2} \right) \right] (1 + |\beta|^2) \end{aligned} \quad (15)$$

$$\begin{aligned} &+ \sqrt{\frac{A}{B}} \left[\cos \frac{\varphi_1 - \varphi_2}{2} \sinh \left(2t\sqrt{AB} \cos \frac{\varphi_1 + \varphi_2}{2} \right) \right. \\ &\quad \left. - \sin \frac{\varphi_1 - \varphi_2}{2} \sin \left(2t\sqrt{AB} \sin \frac{\varphi_1 + \varphi_2}{2} \right) \right] |\alpha| |\beta|, \\ \langle \hat{b}_{out}^+ \hat{b}_{out} \rangle &= \frac{1}{2} \left[\cos \left(2t\sqrt{AB} \sin \frac{\varphi_1 + \varphi_2}{2} \right) \right. \\ &\quad \left. + \cosh \left(2t\sqrt{AB} \cos \frac{\varphi_1 + \varphi_2}{2} \right) \right] |\beta|^2 \\ &\quad + \frac{B}{A} \frac{1}{2} \left[\cosh \left(2t\sqrt{AB} \cos \frac{\varphi_1 + \varphi_2}{2} \right) \right. \\ &\quad \left. - \cos \left(2t\sqrt{AB} \sin \frac{\varphi_1 + \varphi_2}{2} \right) \right] (1 + |\alpha|^2) \\ &\quad + \sqrt{\frac{B}{A}} \left[\cos \frac{\varphi_2 - \varphi_1}{2} \sinh \left(2t\sqrt{AB} \cos \frac{\varphi_1 + \varphi_2}{2} \right) \right. \\ &\quad \left. - \sin \frac{\varphi_2 - \varphi_1}{2} \sin \left(2t\sqrt{AB} \sin \frac{\varphi_1 + \varphi_2}{2} \right) \right] |\alpha| |\beta|, \end{aligned} \quad (16)$$

Where $|\beta|^2 = (\pi \epsilon_0 c \hbar / 2 \omega_1) (r G_S / \mu_{10})^2$, and $G_S \propto \sqrt{2 / \epsilon_0 \hbar N} \mu^2 \rho_{SWM}^{(5)}$.

Figure 6(a) shows an inverted-V-type four-level atomic system for simultaneously producing FWM and SWM processes which are used as the “first” nonlinear process. By scanning Δ_2 with a fixed Δ_3 and different Δ_1 , Figs. 6(b) and 6(c) show the measured FWM signal in the Stokes channel and SWM signal in the anti-Stokes channel, respectively. Due to the crucial condition of the three-photon resonance of SWM process, SWM signal occurs in a narrow region which is inside the linewidth of the fluorescence. However, the cascaded-signal of the FWM process is not observed due to the strong dressing effect of E_3 and E'_3 which induce a suppressed dip in the anti-Stokes signal, while the one of the SWM process is very weak due

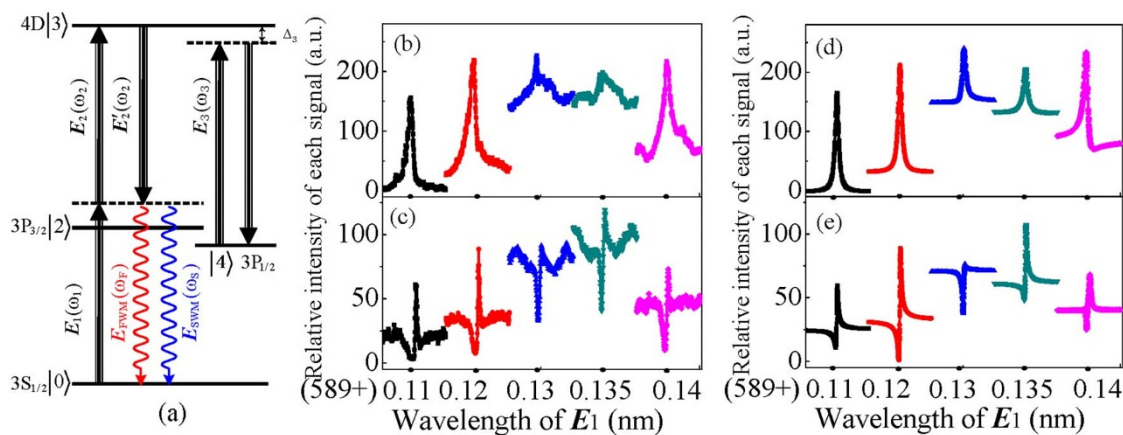


Figure 6 | (a) An inverted-V-type four-level atomic system for producing FWM and SWM processes. The amplified (b) FWM signal in Stokes channel and (c) SWM signal in anti-Stokes channel measured at output of amplifier. (d) and (e) are the corresponding theoretical simulations based on Eqs. (15) and (16).

to the low efficiency of fifth-order nonlinear process. Taking the dressing effect into account, we show the theoretical results in Figs. 6(d) and 6(e) which agree well with the experiment.

In summary, we have theoretically and experimentally studied the parametric amplification process of MWM signal and CNP, both of which are made up of a conventional phase conjugate MWM process and a self-diffraction FWM process. The common pumping beam of these two processes is laser or ASE. For laser pumping case, the SD-FWM process serves as a quantum linear amplifier seeded by the “first” nonlinear MWM process and a CNP because the quantum properties are destroyed by resonant effects. For the ASE pumping case, only the CNP occurs. In both the two cases, the MWM signals in the “first” process have the same linewidths due to the selected effect of its EIT window while that of the “second” process is much narrower than the corresponding result of the “first process” due to the second selected effect of its EIT window. In addition, the PSA process seeded by two MWM processes, and CNP constituted of a SWM process and a FWM process have also been presented.

Methods

Experiment procedure. Two MWM processes are used to implement this phenomenon. To produce the seeded FWM signal E_F , two dye lasers (Narrowscan, 0.04 cm^{-1} linewidth) pumped by an injection locking single mode Nd:YAG laser (Continuum Powerlite DLS 9010, 10 Hz repetition rate, 5 ns pulsewidth) are used to respectively generate the pumping field E_1 and driving fields E_2 and E'_2 with frequency ω_i and frequency detuning $\Delta_i = \omega_{mn} - \omega_i$ ($i = 1, 2$), where ω_{mn} denotes the corresponding transition frequency. They satisfy the phase-matching condition $\mathbf{k}_F = \mathbf{k}_1 + \mathbf{k}_2 - \mathbf{k}'_2$ (\mathbf{k}_i denotes the wave vector of the corresponding electric field), where the pumping beam E_1 can be either a laser beam (E_{1L}) or an ASE beam (E_{1A}). According to the third-order nonlinear susceptibility $\chi^{(3)}$, FWM signal E_F has an orthogonal linear polarization with pumping field E_1 because driving fields E_2 and E'_2 are set at an orthogonal polarization configuration. Generated FWM signal E_F counterpropagates with the field E'_2 , detected by a fast detector via a collecting lens and a fast gated integrator (gate width of 50 ns) as shown in Fig. 1, which has a small angle θ against to the direction of counterpropagating beams E_1 and E_2 . Then, by blocking E_2 and E'_2 as shown in Fig. 1(b), the so-called conical emission⁷ is observed. Such process is well interpreted by a SD-FWM process, in which a strong pumping field E_1 is mixed with two weak fields E_S and E_{aS} , satisfying $\mathbf{k}_S = 2\mathbf{k}_1 - \mathbf{k}_{aS}$ and $\mathbf{k}_{aS} = 2\mathbf{k}_1 - \mathbf{k}_S$, respectively.

PA-MWM. The SD-FWM process serving as quantum linear amplifier is prepared outside the resonant region of sodium D2 transition. Then, by applying two driving fields into upper levels, another FWM, the propagating direction of which can be controlled by the phase-matching condition, is seeded into the Stokes channel of SD-FWM process. Two detectors are put along the hypotenuse of conical emission symmetrically with respect to the pumping beam and record the amplified output signals.

CNP. CNP occurs in the same way as mentioned above except for the position of the pumping field frequency. By scanning the grating of laser device in a wide range, two kinds of pumping fields (laser and ASE) are obtained successively. For laser case, a

SD-FWM process occurs inside the resonant region of sodium D2 transition, where the quantum property of two generated beams is destroyed. For ASE case, the D2 transition is coupled by ASE, where two ASE-FWM processes are cascaded.

- Kolleck, C. Cascaded second-order contribution to the third-order nonlinear susceptibility. *Phys. Rev. A* **69**, 053812 (2004).
- Dolgaleva, K., Shin, H. & Boyd, R. W. Observation of a microscopic cascaded contribution to the fifth-order nonlinear susceptibility. *Phys. Rev. Lett.* **103**, 113902 (2009).
- Zheng, H., Zhang, J. & Xiao, M. Controlling cascade third-order and fifth-order nonlinear optical processes via atomic coherence. *OSA. Cleo. QELS. JTUD8* (2010).
- Pooser, R. C., Marino, A. M., Boyer, V., Jones, K. M. & Lett, P. D. Low-noise amplification of a continuous variable quantum state. *Phys. Rev. Lett.* **103**, 010501 (2009).
- Corzo, N. V., Marino, A. M., Jones, K. M. & Lett, P. D. Noiseless optical amplifier operating on hundreds of spatial modes. *Phys. Rev. Lett.* **109**, 043602 (2012).
- Boyer, V., Marino, A. M., Pooser, R. C. & Lett, P. D. Entangling light in its spatial degrees of freedom with four-wave mixing in an atomic vapor. *Chem. Phys. Chem.* **10**, 755–760 (2009).
- Boyer, V., Marino, A. M., Pooser, R. C. & Lett, P. D. Entangled images from four-wave mixing. *Science* **321**, 544–547 (2008).
- Levenson, J. A., Abram, I. & Rivera, Th. Reduction of quantum noise in optical parametric amplification. *J. Opt. Soc. Am. B.* **10**, 2233 (1993).
- Kumar, P. & Kolobov, M. I. Degenerate four-wave mixing as a source for spatially-broadband squeezed light. *Opt. Comm.* **104**, 374–378 (1994).
- Zhang, Y., Khadka, U., Anderson, B. & Xiao, M. Temporal and spatial interference between four-wave mixing and six-wave mixing channels. *Phys. Rev. Lett.* **102**, 013601 (2009).
- Lukin, M. D., Matsko, A. B., Fleischhauer, M. & Scully, M. O. Quantum noise and correlations in resonantly enhanced wave mixing based on atomic coherence. *Phys. Rev. Lett.* **82**, 1847–1850 (1999).
- Lukin, M. D., Hemmer, P. R. & Scully, M. O. Resonant nonlinear optics in phase-coherent media. *Adv. Atom Mol. Opt. Phys.* **42**, 347–386 (2000).
- McCormick, C. F., Marino, A. M., Boyer, V. & Lett, P. D. Strong low-frequency quantum correlations from a four-wave mixing amplifier. *Phys. Rev. A*, **78**, 043816 (2008).
- Jasperse, M., Turner, L. D. & Scholten, R. E. Relative intensity squeezing by four-wave mixing with loss: an analytic model and experimental diagnostic. *Opt. Express*, **19**, 3765–3774 (2011).

Acknowledgments

This work was supported by the 973 Program (2012CB921804), NSFC (11104216, 10974151, 61078002, 61078020, 11104214, 61108017, 61205112), NCET (08-0431), RFD (20110201110006, 20110201120005, 20100201120031), FRFCU (2012jdhz05, 2011jdhz07, xjj2011083, xjj2011084, xjj2012080, xjj2013089), and CPSF (2012M521773).

Author contributions

H.B.Z., C.B.L., and Y.P.Z. provided the idea and main contributions to the theoretical and experimental analysis of this work. X.Z., Z.Y.Z., Y.L.T., and H.X.C. contributed to the presentation and execution of the work. All authors discussed the results and contributed to writing the manuscript.



Additional information

Competing financial interests: The authors declare no competing financial interests.

License: This work is licensed under a Creative Commons Attribution-NonCommercial-NoDerivs 3.0 Unported License. To view a copy of this license, visit <http://creativecommons.org/licenses/by-nc-nd/3.0/>

How to cite this article: Zheng, H. *et al.* Parametric Amplification and Cascaded-Nonlinearity Processes in Common Atomic System. *Sci. Rep.* 3, 1885; DOI:10.1038/srep01885 (2013).